

T1044-2017 sPHENIX Test Beam EMCal Analysis

Joe Osborn¹ and Jin Huang²¹ University of Michigan²Brookhaven National Laboratory

November 7, 2017

Abstract

This document is intended to support the material associated with the 2017 sPHENIX test beam analysis associated with the EMCal. The 2017 test beam was the first to use 2D projective SPACAL towers and is designed for covering the high rapidity region of $\eta \sim 1$ at sPHENIX. Data was collected both as a function of energy and position to try and determine effects from the block boundaries of the EMCal. Final linearity and resolution plots are shown at the end of the note for the beam centered on a particular tower. The resolution for the entire EMCal will also be shown and conclusions will be drawn regarding the functionality of this EMCal and thus the data that was taken.

Contents

1	Introduction	3
2	Analysis Code and Methods	3
2.1	Software Documentation	3
2.2	Data Sets	3
2.3	Analysis Cuts	4
2.4	Hodoscope Position Dependent Correction	4
2.5	Cluster Position Dependent Correction	13
3	Simulations	15
3.1	Simulation Resolution	16
3.2	Constructing Position Dependent Corrections in Simulation for Data	18
3.2.1	Matching Simulation and Data	18
4	Results and Conclusions	22
4.1	First Joint Energy Scan Results	22
4.2	Third Joint Energy Scan Results	23
4.3	Conclusions	24
4.4	Final Linearity and Resolution	25

List of Figures

2.1	Resolution and linearity in the first joint energy scan with a 1x1 hodoscope cut. . . .	5
2.2	Resolution and linearity in the first joint energy scan with a 5x5 hodoscope cut. . . .	5
2.3	Energy response in the first joint energy scan as a function of hodoscope position . .	6
2.4	Example energy responses as a function of hodoscope finger	7
2.5	Energy response as a function of hodoscope position after recalibration	8
2.6	Resolution and linearity after hodoscope recalibration from the first joint energy scan	8
2.7	Energy response as a function of hodoscope in the third joint energy scan for an 8 GeV beam.	9
2.8	Energy response as a function of hodoscope after recalibration in the third joint energy scan for an 8 GeV beam.	10
2.9	Resolution of the third joint energy scan after hodoscope recalibration with a 2% beam spread term	10
2.10	Energy responses from the first joint energy scan after the hodoscope recalibration .	11
2.11	Energy responses from the third joint scan after the hodoscope calibration	12
2.12	Energy responses from the third joint energy scan with reduced fit ranges	12
2.13	Energy responses as a function of ϕ and η before cluster position recalibration. . . .	13
2.14	Energy responses as a function of ϕ and η after cluster position recalibration. . . .	14
2.15	Resolution from the first joint energy scan with cluster position correction	14
2.16	Resolution from the third joint energy scan with cluster position correction	15
3.1	An image showing an electron event with the 0° , i.e. nominal, beam tilt in simulation.	16
3.2	Simulated linearity and resolution after position dependent energy response correction for a 0° tilted electron beam.	17
3.3	An image showing an electron event with the 10° beam tilt in simulation.	17
3.4	Simulated linearity and resolution after position dependent energy response correction for a 10° tilted electron beam.	17
3.5	Reconstructed cluster energy in simulation and data	19
3.6	Reconstructed cluster energy in simulation and data	19
3.7	Position dependent energy responses in data and simulation are matched together for the purposes of taking a ratio.	20
3.8	Position dependent energy responses in data and simulation are matched together for the purposes of taking a ratio.	21
3.9	The ratio of simulation and data is shown for the position dependent energy response. The ratio is not flat, indicating that significant tuning is required in the simulation to accurately represent the real calorimeters energy response as a function of position.	21
4.1	First joint energy scan resolution with cluster position dependent correction	22
4.2	First joint energy scan resolution with hodoscope position correction	23
4.3	Third joint energy scan resolution with cluster position dependent correction	23
4.4	Third joint energy scan resolution with hodoscope position correction	24
4.5	Linearity of the EMCal in the first joint energy scan.	25
4.6	Resolution of the EMCal in the first joint energy scan.	26

1 Introduction

The 2017 T-1044 test beam was designed to be the first test of the high rapidity $\eta \sim 1$ sPHENIX calorimetry. In particular, the EMCal tested was the first with 2D projective tungsten scintillating fiber towers produced, and thus the test beam was a first step in understanding the 2D projective towers. It is also the first sPHENIX test beam with blocks containing the 2x2 tower configuration that sPHENIX intends to build. Nearly all of the test beam details are documented in the wikipedia page:

https://wiki.bnl.gov/sPHENIX/index.php/2017_calorimeter_beam_test

Since this was the first high rapidity EMCal, there was emphasis in the data collection to study and understand the effects of the block boundaries. The effect of the block boundaries was quantified by performing energy scans covering either one single tower and several towers to include the effects of the block boundaries. To quantify these effects, position dependent energy responses were made for these runs. These responses could then be used as recalibrations to the overall energy response, depending on where the electron showered. This procedure will be documented here, in addition to the various analysis cuts and methods used to construct final results.

2 Analysis Code and Methods

2.1 Software Documentation

Wikipedia pages documenting test beam information, and analysis can be found at Refs. [4, 3]. A wikipedia page documenting various EMCal meeting presentations and other information regarding the 2017 EMCal analysis can be found at Ref. [2]. The code used for this analysis is located in the sPHENIX github repository. All of the code can be found in Ref. [5]. Code and macros used for analyzing the data and constructing the position dependent corrections can be found in the subsequent directories within github in ShowerCalib/ and ShowerCalib.PositionDependent/. Any additional code can be found in /sphenix/user/jdosbo/Prototype3/.

It should also be noted that the position dependent energy correction is the same as what was implemented in the full sPHENIX barrel simulations. This acts on the clusters after the initial clustering calibration, and can be found in the sPHENIX github repository [6].

2.2 Data Sets

In general this note documents the analysis of two sets of runs, which will be referred to as the “first joint energy scan” and the “third joint energy scan.” The two sets of runs are different in that the first joint energy scan has the electron beam centered on a 4x4 cm area in one tower, while the third joint energy scan uses a wider beam spread to cover a larger area of the calorimeter to investigate effects from block boundaries. The first joint energy scan contains run numbers 3736-3751, while the third joint energy scan contains run numbers 3989-4010. This is documented on the wikipedia pages mentioned above. The calibrated DSTs that are analyzed throughout this note can be found

in the following directory on RCF:

/sphenix/data/data01/t1044-2016a/production.2017/Production_0216.UpdateCalib/beam_*.root

2.3 Analysis Cuts

Analysis cuts can be found in the code package /ShowerCalib/ as discussed above. The cuts are elaborated on here.

Only runs that passed electron cuts were analyzed. The only cut which was required was that there be a “good_e” cut, i.e. good electron. This required that there be a valid hodoscope hit in both the vertical and horizontal fingers, or that in each direction the energy measured in the hodoscope was greater than a threshold ADC of 30. The “good_e” cut also required that the Cherenkov energy sum was greater than an energy threshold of 100 as a function of the truth electron beam energy. These cuts were utilized in order to suppress both background from MIPs as well as hadron contamination in the beam. After these cuts were implemented, a simple clustering algorithm was performed to determine the energy response as well as cluster ϕ, η position.

Clustering was performed with a simple algorithm. Both 3x3 and 5x5 clusters were constructed, where the 3x3 and 5x5 simply refer to the number of towers included in the clustering algorithm. The tower with the maximum energy was determined for a particular event. From that tower, the energy response was determined to be the total calibrated energy sum in a 3x3 or 5x5 tower square around the maximum energy tower. The cluster ϕ and η position were determined with an energy weighted average in that 3x3 or 5x5 tower square. Calibrated tower energies were determined offline via MIP calibrations as was done in the previous 2016 test beam [1]. Recalibrated energies using the hodoscope or position dependence of the cluster are described in further detail below.

2.4 Hodoscope Position Dependent Correction

The hodoscope position dependent correction was first used in Ref. [1]. While the sPHENIX barrel will not be lined with hodoscopes, the hodoscope is used in the test beam for accurate identification of the beam position. The hodoscope is installed upstream of the EMCal detector; a full description of the hodoscope is in Ref. [1]. Here, the hodoscope fingers are used to identify the position of the cluster; then a position dependent energy correction is constructed based on the position identified in the hodoscope. Before this correction is implemented, the dependence on the hodoscope fingers can visually be seen by requiring a cut on the hodoscope finger around the cluster. For example, a 1x1 hodoscope cut around the 1x1 finger that produces the best energy response results in the resolution shown in figure 2.1. If we expand the cut and included the 5x5 fingers around the best energy response, the resolution degrades considerably as can be seen in figure 2.2. This behavior can also be seen in figure 2.3, which shows the average energy response on the z axis versus the horizontal and vertical hodoscope positions for a 8 GeV electron. Clearly the response is highly dependent on the position of the electron.

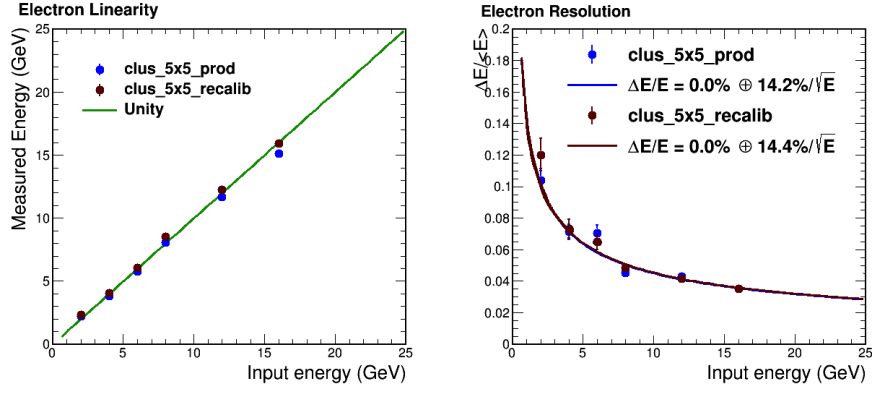


Figure 2.1: Resolution and linearity in the first joint energy scan with a 1x1 hodoscope cut.

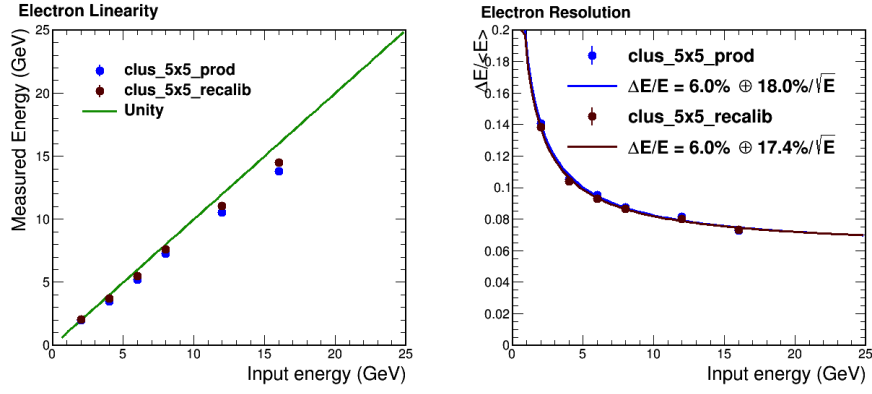


Figure 2.2: Resolution and linearity in the first joint energy scan with a 5x5 hodoscope cut.

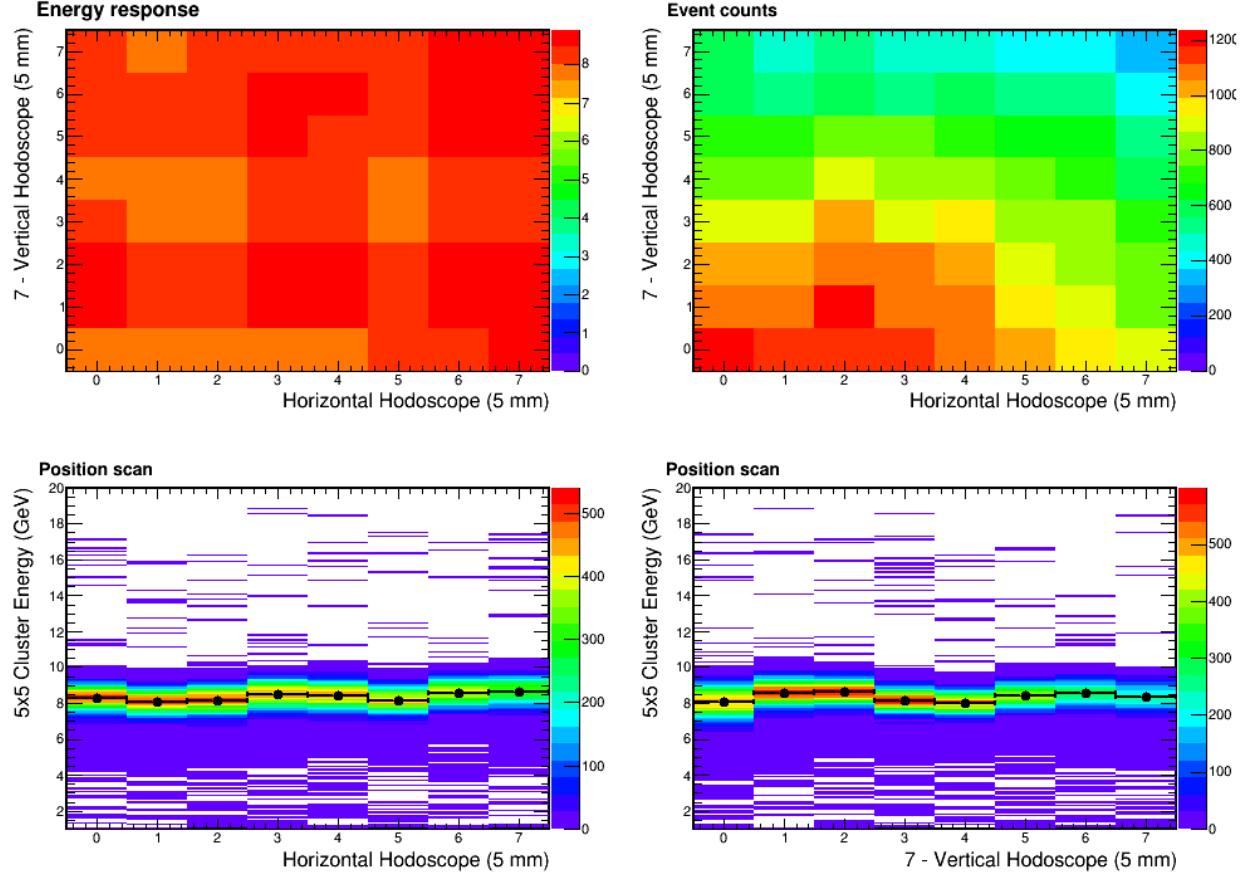


Figure 2.3: The energy response in the first joint energy scan as a function of hodoscope position for an 8 GeV electron beam, shown as the mean electron response in 2D hodoscope bins in the top left and as two separate 2D histograms in the bottom left and bottom right.

To correct for this position dependence, the energy response as a function of the 8x8 hodoscope fingers is constructed. The 8 GeV data is used to perform the correction since the beam spread should cover all 64 hodoscope fingers while the energy is high enough to avoid any backgrounds from noise. The energy response was plotted as a function of the 64 hodoscope fingers. Examples of the responses can be seen in figure 2.4 for horizontal hodoscope 4 and all vertical hodoscopes. Each energy response was fit to a Gaussian function, and the mean was extracted from the fits. The energy correction for that particular horizontal+vertical hodoscope finger is then simply $8/\mu$, where μ is the mean from the Gaussian fit. This gives 64 recalibration constants, one for each hodoscope finger. These constants can then be applied to the total cluster energy response to improve the resolution of the EMCal. The same figure as figure 2.3 is shown after the recalibration is applied in figure 2.5. The effect of the recalibration is clear in that all of the responses are centered at nearly 8 GeV for each hodoscope finger.

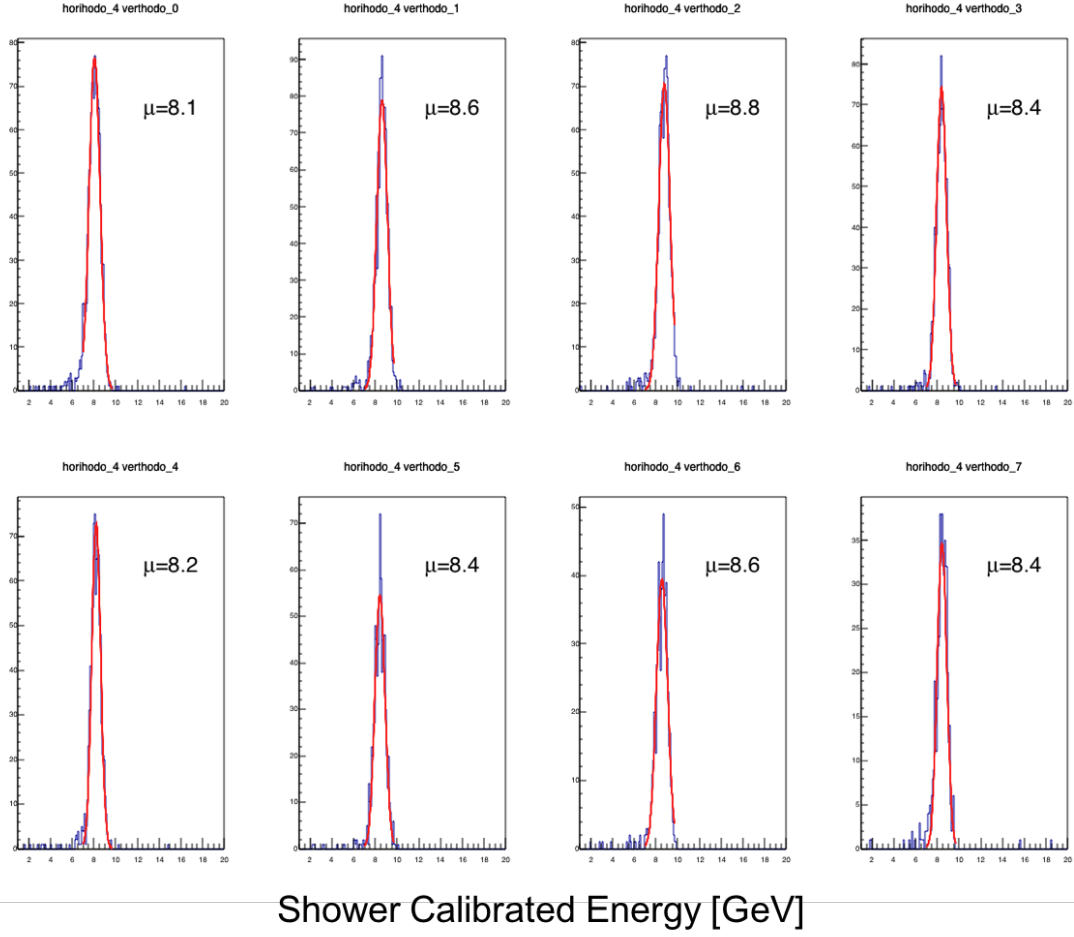


Figure 2.4: Example energy responses as a function of hodoscope finger for an 8 GeV electron beam in the first joint energy scan.

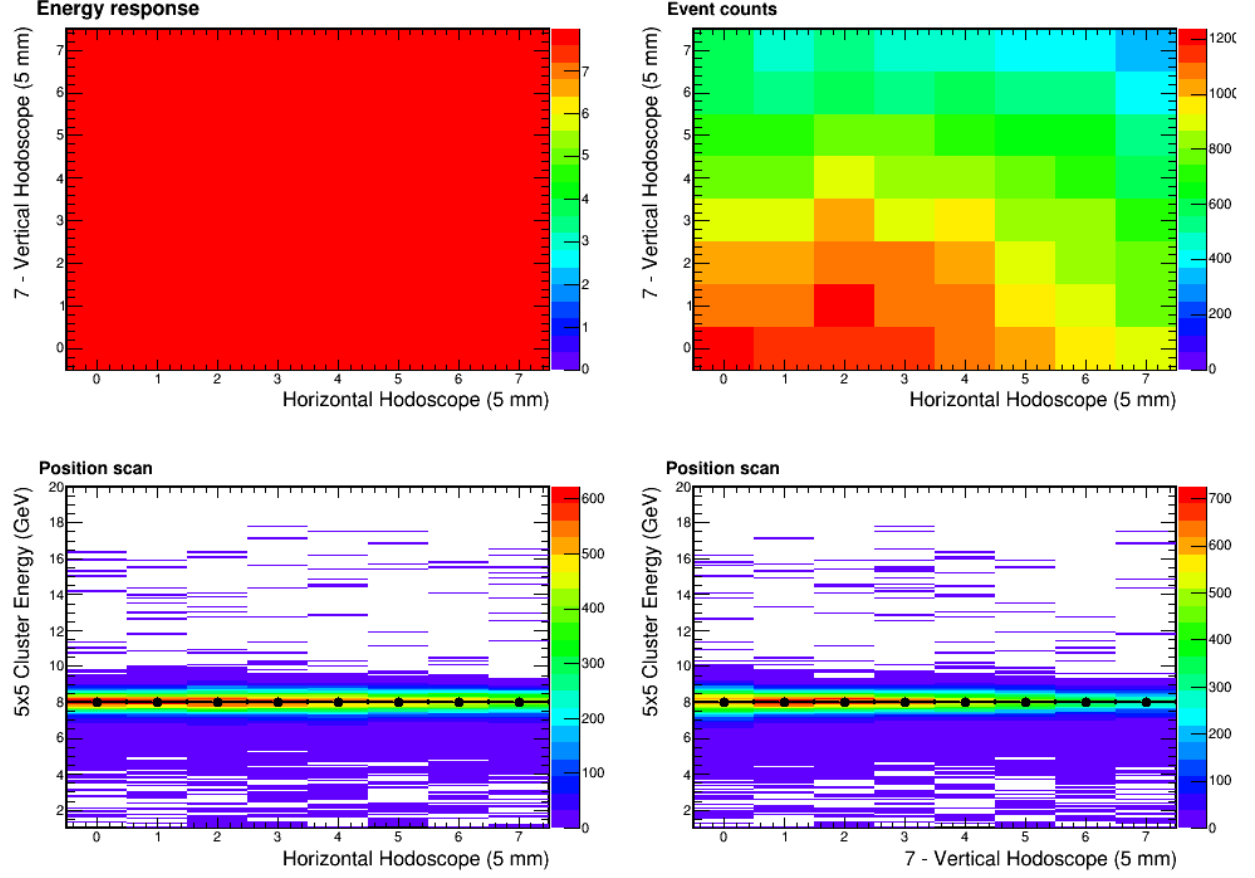


Figure 2.5: Energy response from the first joint energy scan as a function of hodoscope position for an 8 GeV electron beam after the recalibration is performed.

The effect of the recalibration on the other energies determines the improvement in the resolution; this is shown in figure 2.6. The resolution from the production values (blue points) is noticeably worse than the resolution after the recalibration is performed (brown points). The simulations curves will be described in more detail later in the note.

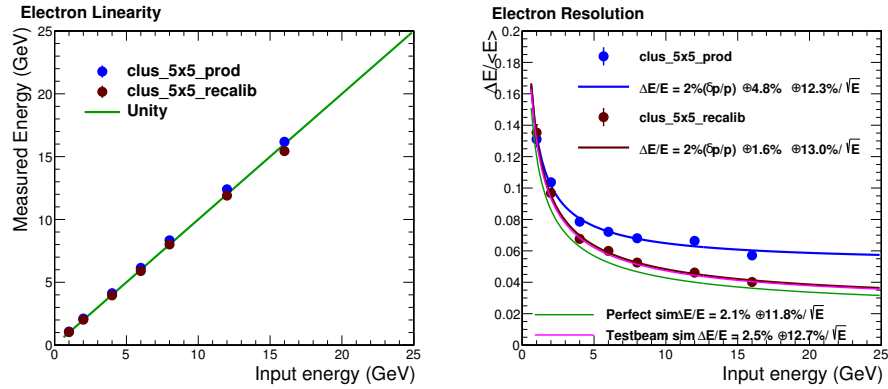


Figure 2.6: Resolution and linearity from the first joint energy scan after the hodoscope recalibration constants are applied, with a 2% beam momentum spread added.

The same procedure can be applied to the third joint energy scan. Note that this procedure is dependent on the beam characterization, so it needs to be repeated for each “set” of runs, e.g. the first versus third joint energy scans which focus on different areas of the calorimeter. The same plots are shown below in figures 2.7, 2.8, 2.9 for the third joint energy scan, documenting the effectiveness of the hodoscope recalibration. It is clear from the resolution that the effect of the block boundaries is quite large. Comparing figures 2.6 and 2.9, we see that the inclusion of the block boundaries degrades the constant term by roughly 2.5%, while the stochastic term is about 1.5% worse.

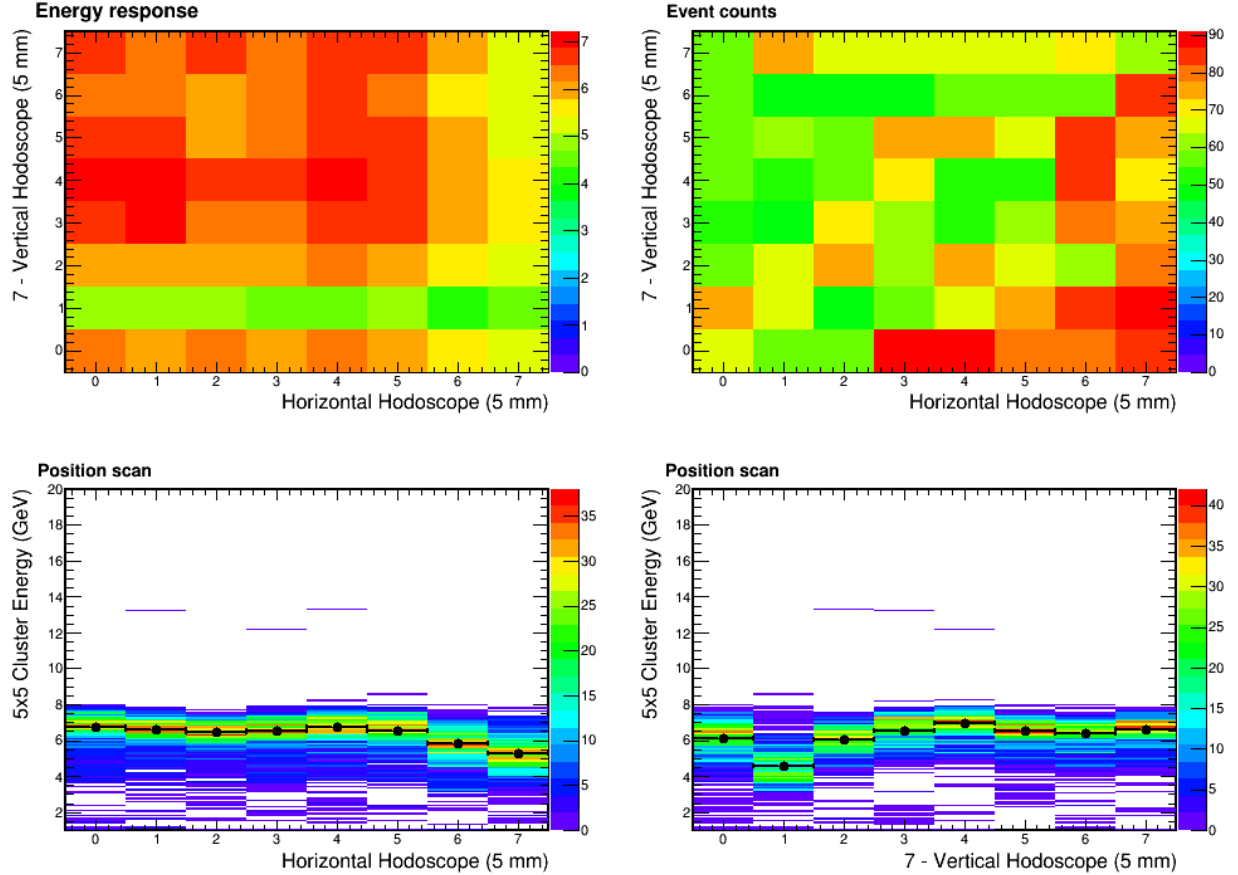


Figure 2.7: Energy response as a function of hodoscope in the third joint energy scan for an 8 GeV beam.

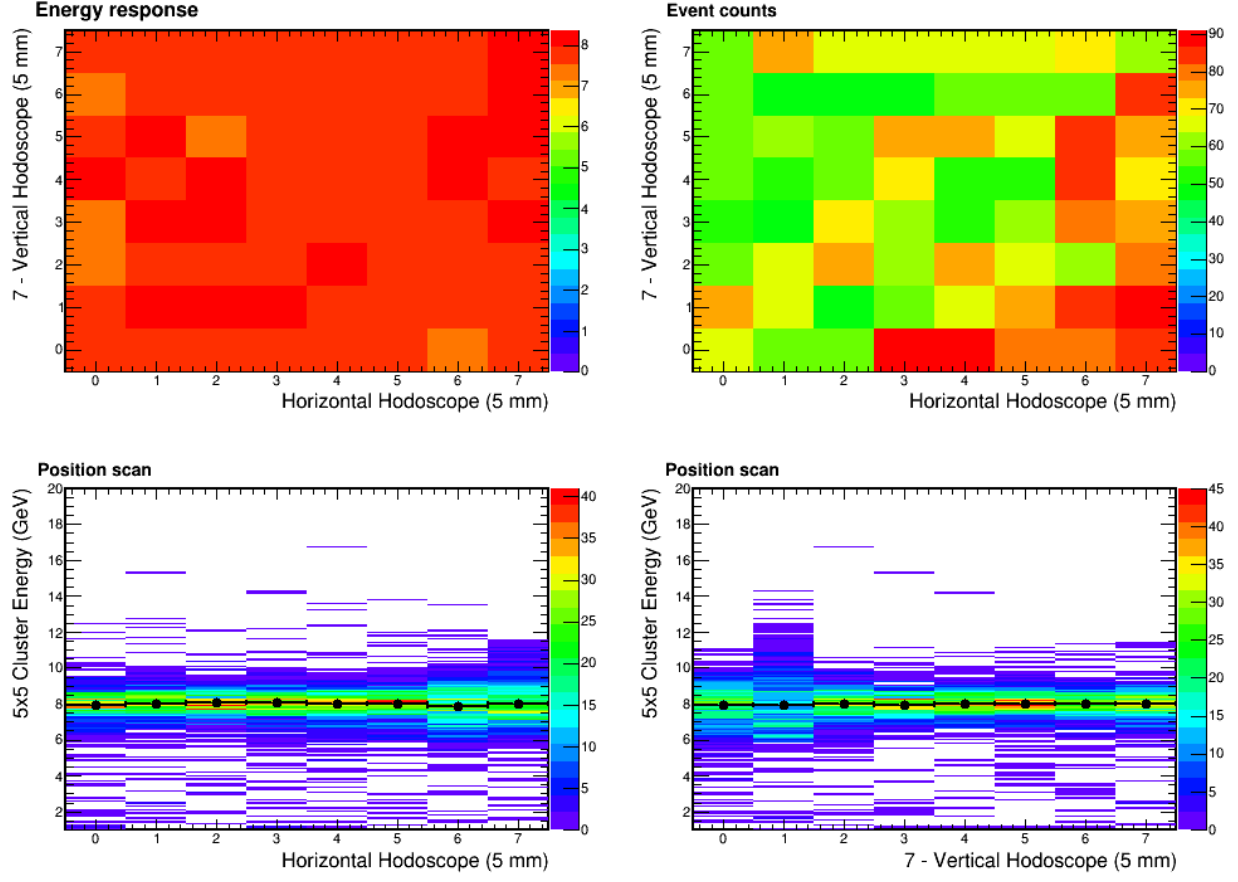


Figure 2.8: Energy response as a function of hodoscope after recalibration in the third joint energy scan for an 8 GeV beam.

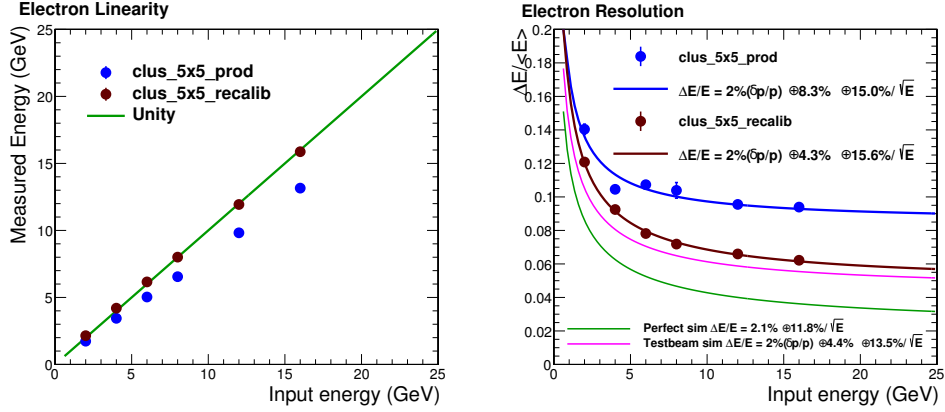


Figure 2.9: The resolution of the third joint energy scan after the hodoscope recalibration with a 2% beam momentum spread term added.

One note should be made that the hodoscope calibration does not entirely clean up the energy responses; namely there are still tails to the energy distributions. Figures 2.10 and 2.11 show the

energy responses from the first joint energy scan and third joint scan, respectively. It is clear from the fits that there are still some low/high energy tails that alter the fit functions, most considerably in the third joint energy scan. Since these are not indicative of the actual peak position, to extract the resolution the fits were altered to better encapsulate the core Gaussian region. In the first joint energy scan data figure 2.10, the fits already capture the peak position well, while in the third joint energy scan data figure 2.11 the reduced fit region is more important due to the more pronounced tails.

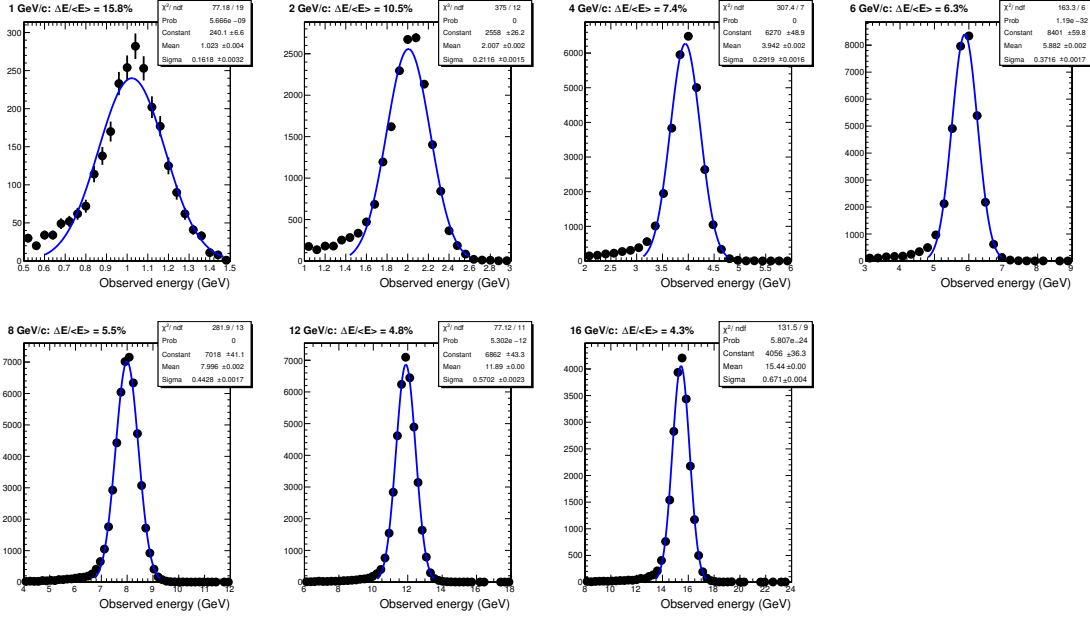


Figure 2.10: Energy responses from the first joint energy scan after the hodoscope recalibration. The responses are mostly evenly distributed around the nominal beam energy, although there is still some low/high energy tail as can be seen from the Gaussian fits.

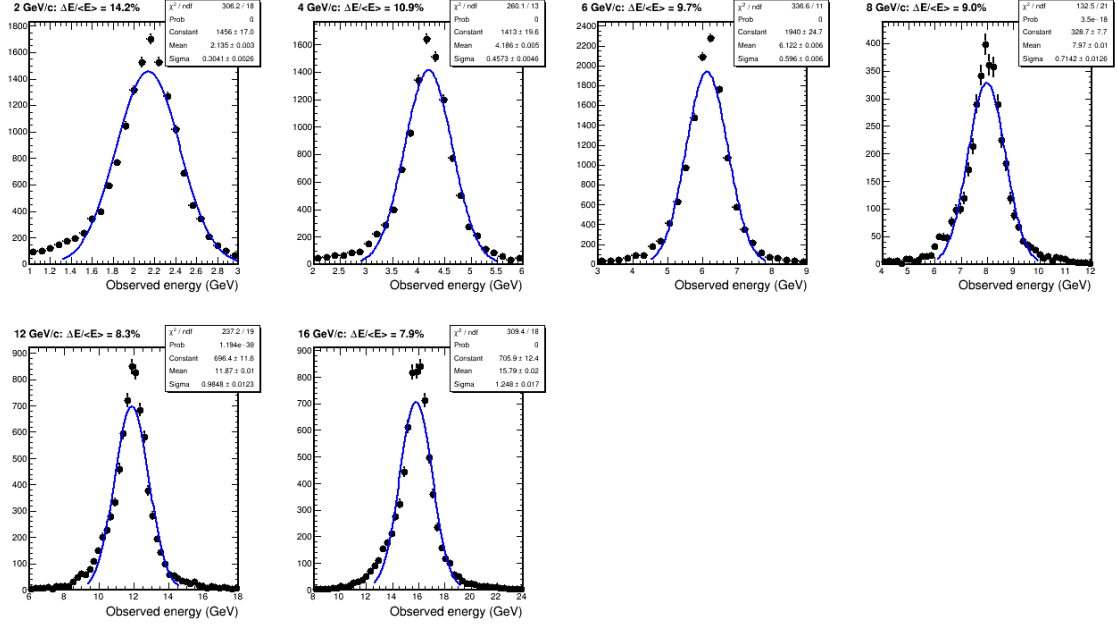


Figure 2.11: Energy responses from the third joint energy scan after the hodoscope recalibration. The responses are mostly evenly distributed around the nominal beam energy, although there is still some low/high energy tail as can be seen from the Gaussian fits.

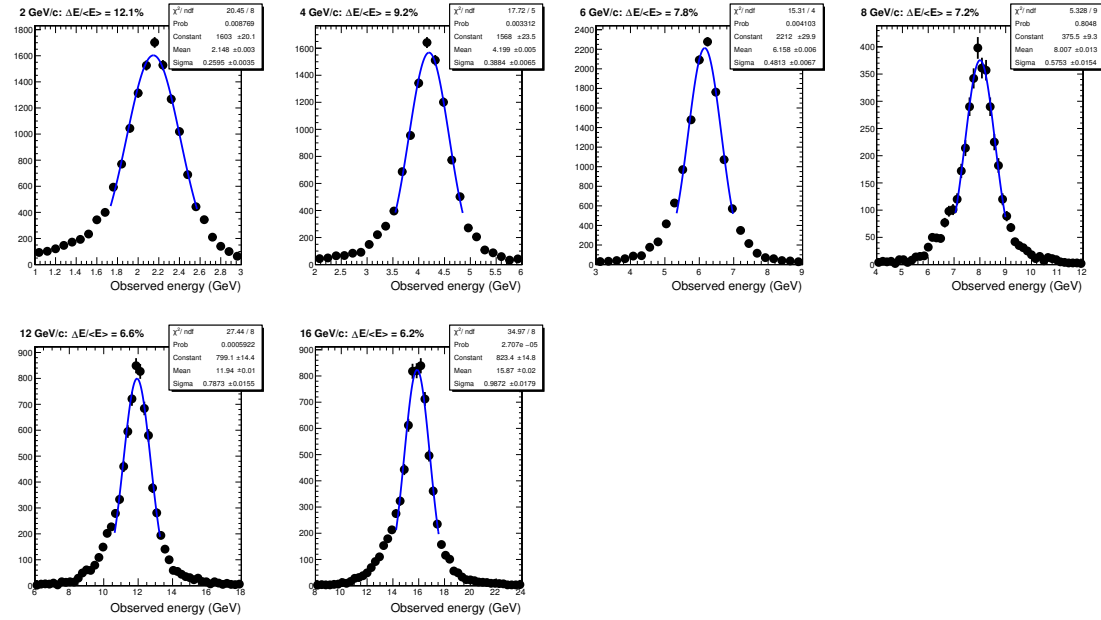


Figure 2.12: Energy responses from the third joint energy scan after the hodoscope recalibration. The fit ranges are reduced to better encapsulate the peak region.

2.5 Cluster Position Dependent Correction

Since the sPHENIX barrel will not be lined with hodoscopes, a different attempt was made to correct for the position dependence of the energy response which did not require the hodoscope. In this correction, the position dependence was quantified with the cluster energy weighted position in ϕ and η . The cluster weighted position was determined in the 2×2 block area in both η and ϕ space, and the energy response was constructed in bins covering the 2×2 block area. With the hodoscope correction, we had an 8×8 finger area determined by the hodoscope to determine 64 calibration constants. This cluster position dependent correction determines the energy response in 16×16 bins covering the area of 4 towers, i.e. in a 2×2 tower block. The energy response was again made in these 16×16 bins and fit to a Gaussian function to determine the calibration constant. The concept is almost identical to the hodoscope position correction; the only difference is that rather than using the hodoscope to identify the position of the electron we use the cluster position to define the position of the electron. The corrections were made, again, for the first and third joint energy scans separately. Here we omit the 8 GeV point from the resolution to avoid any autocorrelations to be present since we are using the actual cluster to determine the energy response.

Example plots for the 12 GeV electron beam data are shown in figures 2.13 and 2.14 before and after the position dependent recalibration is applied in both the ϕ and η cluster direction. Note that the x axes are the cluster ϕ and η positions within a block, where the left edge of the block boundary is at 0 and the right edge of the block boundary is at 2. The edges span a 2×2 tower configuration, which is apparent in the figures as the two areas in each figure where the counts are the largest. Before the recalibration there is a significant position dependence to the energy response, whereas after recalibration the responses across the entire calorimeter are significantly more uniform. These figures are comparable to the hodoscope position dependent recalibrations in the bottom panels of figures 2.3 and 2.5.

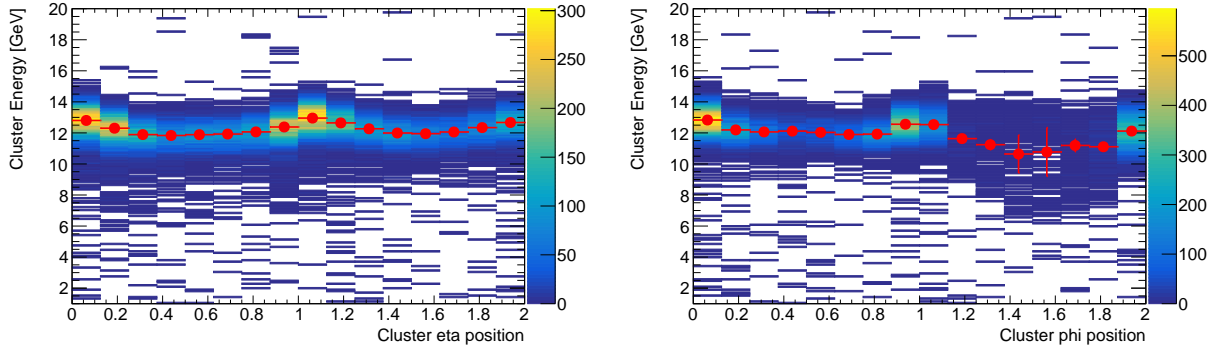


Figure 2.13: The energy response is shown as a function of cluster η (left) and ϕ (right) before the position dependent recalibration is applied for a 12 GeV electron beam.

The linearity and resolution of the first and third joint scans are shown below in figures 2.15 and 2.16, with the cluster position dependent correction applied. The simulation curves in these figures are up-to-date and accurate, and will be described in more detail in the simulation section. There will also be further discussion about why the simulation matches the data well in the first joint energy scan but not in the third joint energy scan. Comparing the resolution parameters from the first joint energy scan with the cluster position correction and hodoscope position correction, figures 2.15 and 2.6 respectively, shows that the resolution curves are very similar. The cluster

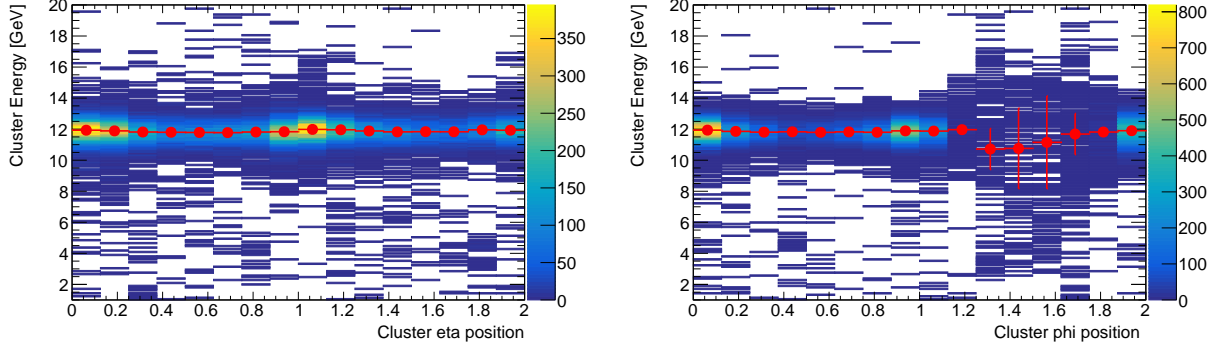


Figure 2.14: The energy response is shown as a function of cluster η (left) and ϕ (right) after the position dependent recalibration is applied. The energy responses are significantly more uniform for a 12 GeV electron beam.

position correction method gives a resolution of $2\%(\delta p/p) \oplus 1.3\% \oplus 13.6\%/\sqrt{E}$, while the hodoscope position correction method gives a resolution of $2\%(\delta p/p) \oplus 1.6\% \oplus 13.0\%/\sqrt{E}$. Here the $(\delta p/p)$ term is a 2% beam momentum spread that is unfolded from the calorimeter resolution. The same conclusion can be drawn for the third joint energy scan. This indicates that when the position correction is made from actual data, the cluster position method is as good as the hodoscope position method. This will be important for calibrating the energy in the sPHENIX detector, since the barrel will not be lined with hodoscopes; this study indicates that with very simple clustering the position energy dependence can be corrected for with the data.

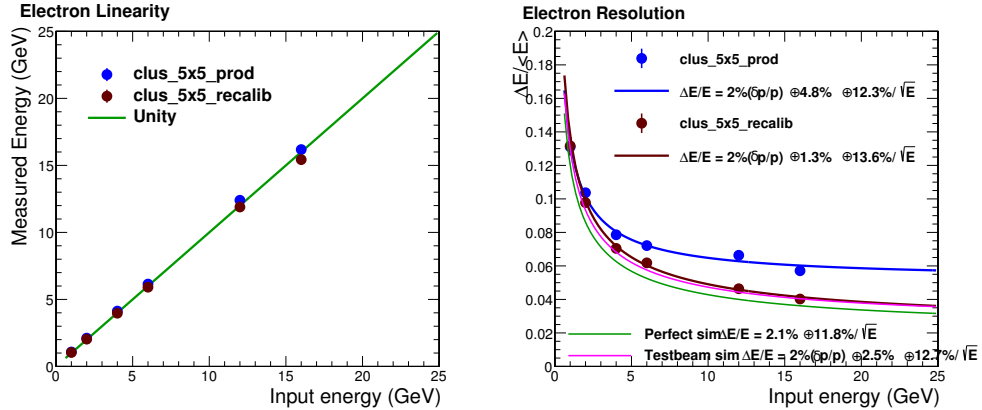


Figure 2.15: The resolution in the first joint energy scan with the application of the cluster position dependent correction is shown. The simulated curves here are up-to-date and accurate, and are described further in the text.

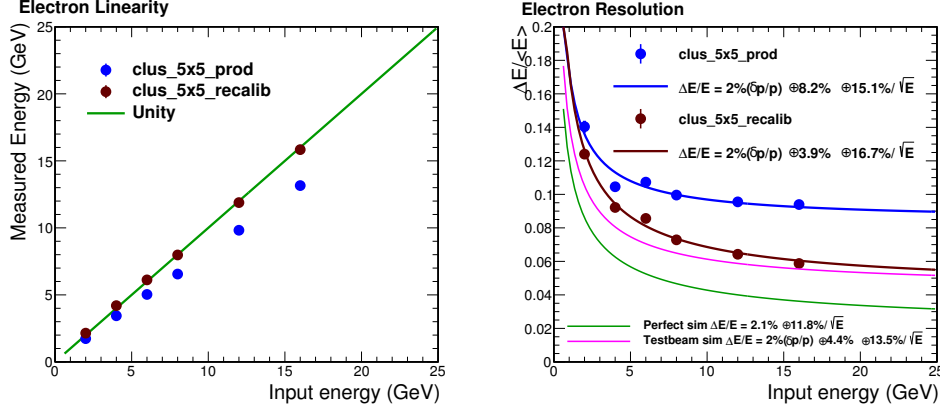


Figure 2.16: The resolution in the third joint energy scan with the application of the cluster position dependent correction is shown. The simulated curves here are up-to-date and accurate, and are described further in the text.

3 Simulations

Simulations were performed with the default Prototype3 testbeam macro, located in /macros/macros/prototype3/. Small modifications to this macro will be discussed in the appropriate subsection. Single electron events were simulated using all Proto3 detectors. The beam characteristics were taken straight out of the GitHub macro. The beam included a 1 millirad angular divergence in both η and ϕ space as well as a 2% momentum smearing which are the same as the actual test beam. Gaussian vertex distributions were used as was in the git macro. A snippet of the code with the beam conditions can be found in the July 18 2017 EMCal presentation, for which links exist at the wiki pages from Section 2. One change that was made offline was to tilt the beam by 10 degrees for the first joint energy scan; this was to match the beam direction as it was in data. In the third joint energy scan, the beam direction was 0 degrees, i.e. square to the face of the calorimeter, so no modification was necessary. The tilt of the beam has important effects on both the positional energy response as well as the overall energy response of the detector, since the 10 degree beam tilt has more radiation lengths to traverse in the EMCal.

The cluster position dependent corrections were also constructed in the simulation as they were in data. These corrections were constructed with a 0 or 10° tilted beam for the two different energy scans, so that the position response would be simulated as similarly as possible to the data. Dedicated simulation runs were performed to construct the corrections, since the beam needed to cover a large area of the calorimeter in order to accumulate enough statistics to perform energy response fits in the 16x16 bins. To achieve this, the beam characteristics in simulation were simply set to cover a large range in z vertex position. The vertex distribution width was set to 10 cm and the vertex distribution function was set to a uniform function rather than a Gaussian function, solely for the purpose of covering a large area of the calorimeter to construct the position dependent correction matrix.

3.1 Simulation Resolution

Simulations were run with a 0 degree beam tilt to compare to the third joint energy scan and a 10 degree tilt for comparison to the first joint energy scan. The same analysis code was used on the simulated data, and resolution and linearity plots were constructed. An image showing an example event in the G4 simulation is shown in figure 3.1 and 3.3 for the 0 and 10° beam tilt, respectively. The procedure is executed the exact same as was done with data; namely the energy response was corrected for as a function of the simulated cluster position as was done in data. The linearity and resolution for 3x3 and 5x5 tower clusters are shown in figures 3.2 and 3.4. The green curve on each plot is the “perfect resolution” of the 2D SPACAL tower in simulation. This curve was determined by firing an electron beam with no momentum or angular spread directly at the center of a single tower. The light collection efficiency was also set to be 100%, so this is the intrinsic electromagnetic energy resolution provided by the ideal SPACAL sampling structure in the simulation.

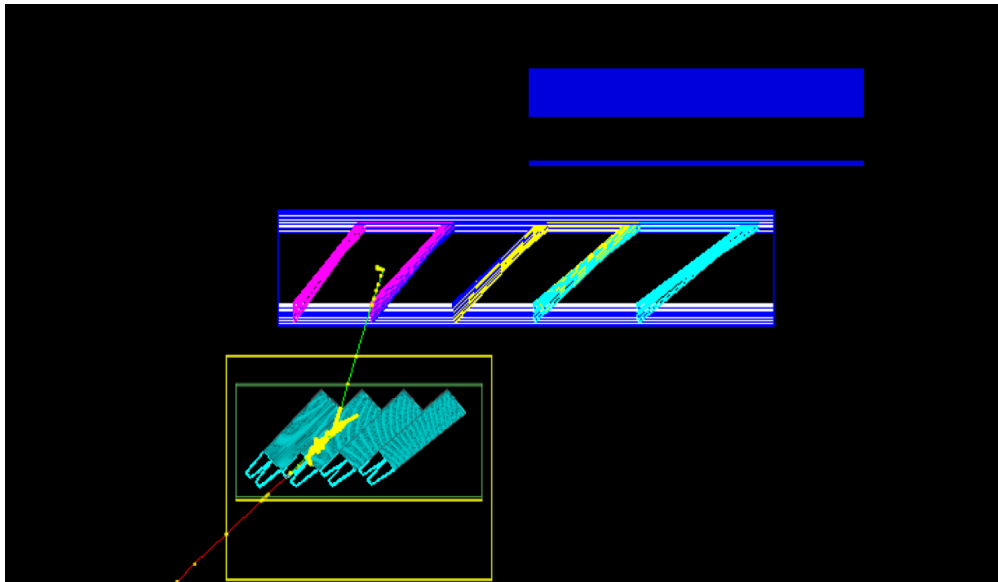


Figure 3.1: An image showing an electron event with the 0°, i.e. nominal, beam tilt in simulation.

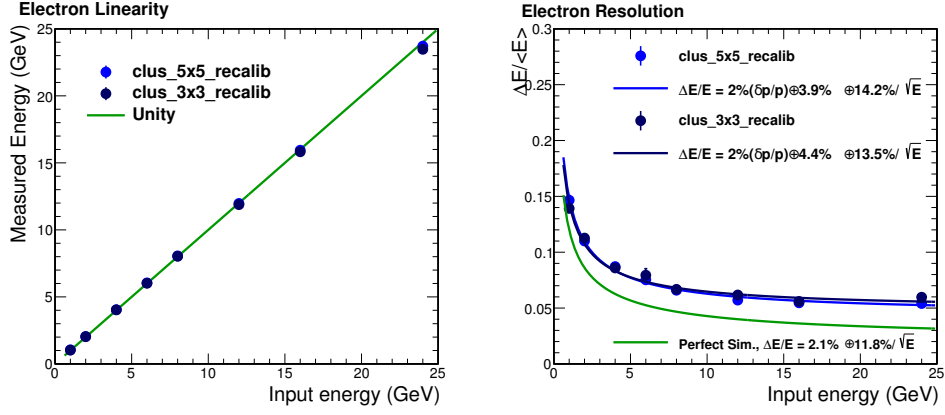


Figure 3.2: Simulated linearity and resolution after position dependent energy response correction for a 0° tilted electron beam.

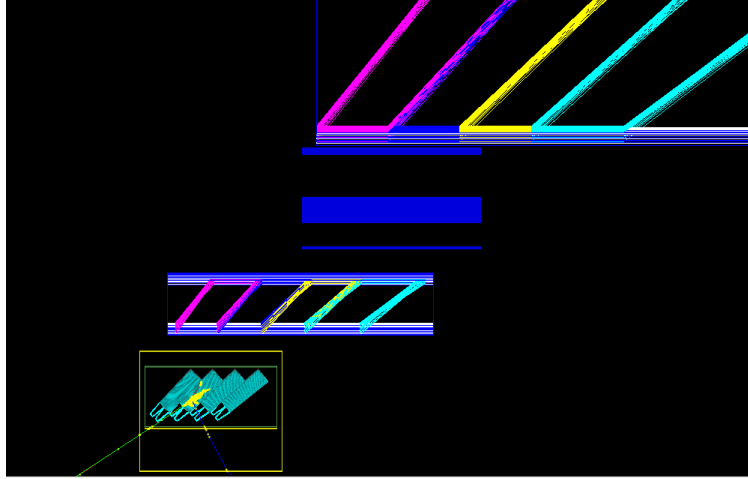


Figure 3.3: An image showing an electron event with the 10° beam tilt in simulation.

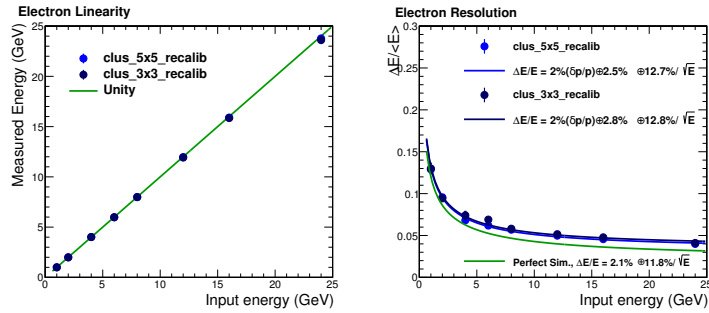


Figure 3.4: Simulated linearity and resolution after position dependent energy response correction for a 10° tilted electron beam.

3.2 Constructing Position Dependent Corrections in Simulation for Data

Ideally we would like to be able to construct the 16x16 position dependent energy correction matrix in simulation and then apply it to the data. In order to do this we need to perform cross-checks that the simulation position dependent energy response actually replicates that of the real data. If it does, then in principle we should be able to construct the correction matrix in the simulation and show that, when applied to the data, the resulting resolution is the same as when the correction matrix is constructed from the data. If the simulation does not replicate the data, then additional tuning of the position dependent energy response would be required.

3.2.1 Matching Simulation and Data

In order to compare the simulation and data, the cluster energy response as a function of the position was plotted. Each slice of the 2D histogram was fit to a Gaussian function in order to make a more visual 1D comparison between the shape of the energy response as a function of the position. To get a more precise comparison of the cluster position, at first the hodoscope position of the electron from data was compared to the truth vertex distribution from the simulation. This is the best and most precise comparison to make to start, since the actual identification of the cluster position could introduce additional smearing into the comparison between simulation and data.

The energy response as a function of the vertical hodoscope position (left, data) and as a function of the y truth vertex position (right, simulation) is shown in figure 3.5. Figure 3.6 shows the perpendicular direction, or the energy response as a function of the horizontal hodoscope position (left, data) and as a function of the z truth vertex position (right, simulation). When comparing the figures, it is important to keep in mind that the simulation shows the response over the entire calorimeter, while the hodoscope only covers about a 4 cm region. The simulation histograms are made in significantly finer bins in order to get a better understanding of the fine structure.

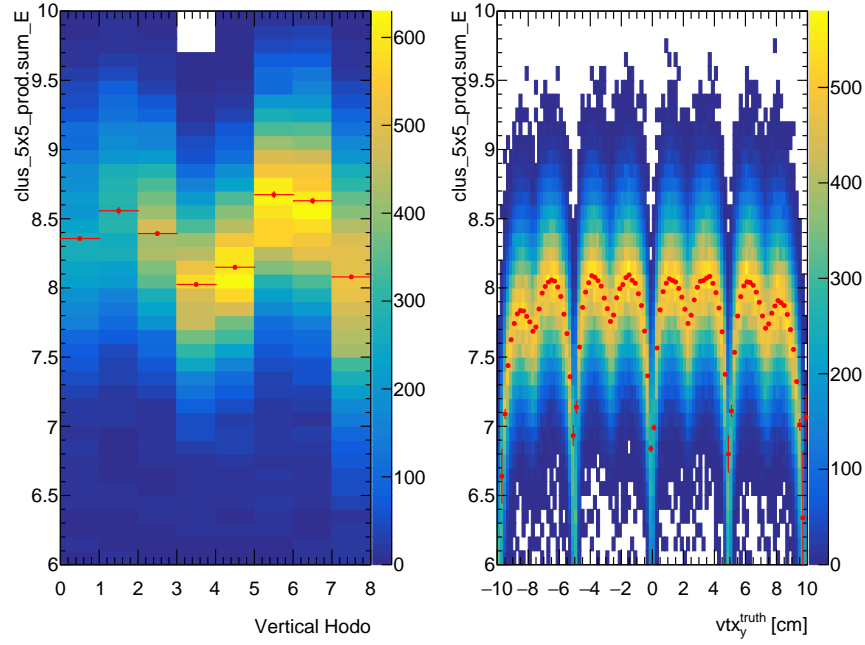


Figure 3.5: The reconstructed cluster energy as a function of the vertical hodoscope position (data, left) and truth y vertex position (right, simulation) is shown. Each slice is fit to a Gaussian function to locate the mean of the distribution.

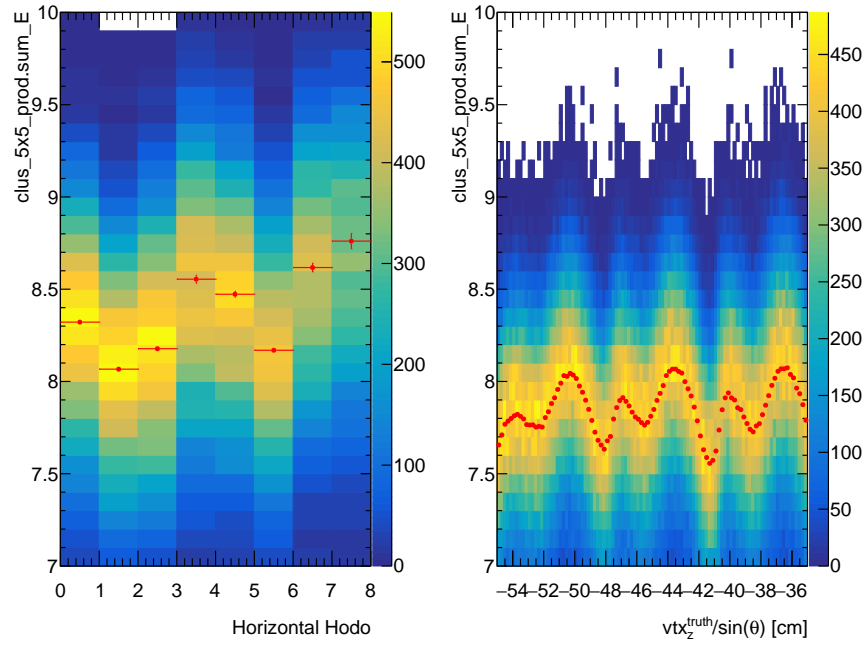


Figure 3.6: The reconstructed cluster energy as a function of the horizontal hodoscope position (data, left) and truth z vertex position (right, simulation) is shown. Each slice is fit to a Gaussian function to locate the mean of the distribution.

To make a more quantitative comparison between the data and the simulation, the red graphs from each histogram were compared as a ratio. If the simulation position dependent energy response replicates the data, then this ratio should be roughly flat. Any constant deviation from unity would simply indicate a calibration difference between the simulation and data, which is not important for comparing the response as a function of the position. Since the hodoscopes do not cover the full calorimeter, while the simulations do, the graphs were overlaid to ensure that the proper regions were being compared. Figures 3.7 and 3.8 show the two graphs overlaid, with the simulation in 1 millimeter bins to ensure that the proper regions are compared. The simulation histogram, and resulting **TGraph**, was remade in 1 cm bins corresponding to the hodoscope fingers to take a ratio. It is clear that the simulation does not accurately emulate the data in terms of the energy response as a function of position from figures 3.7 and 3.8. This is shown by taken the ratio between data and simulation for both horizontal and vertical directions, shown in figure 3.9, which is clearly not flat.

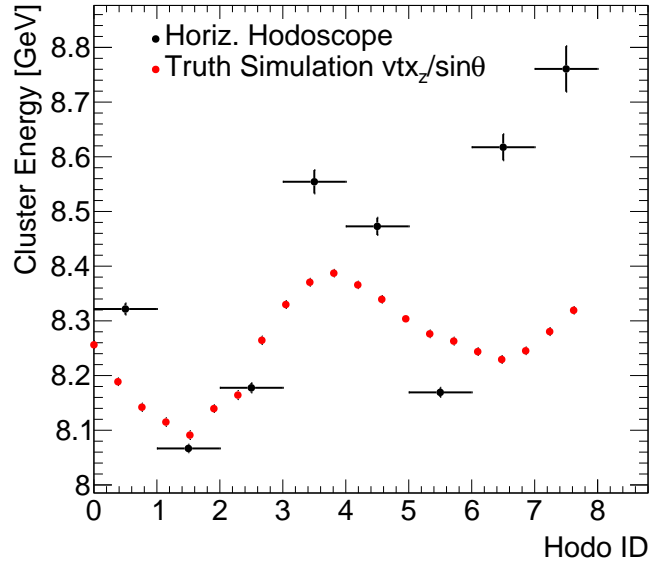


Figure 3.7: Position dependent energy responses in data and simulation are matched together for the purposes of taking a ratio.

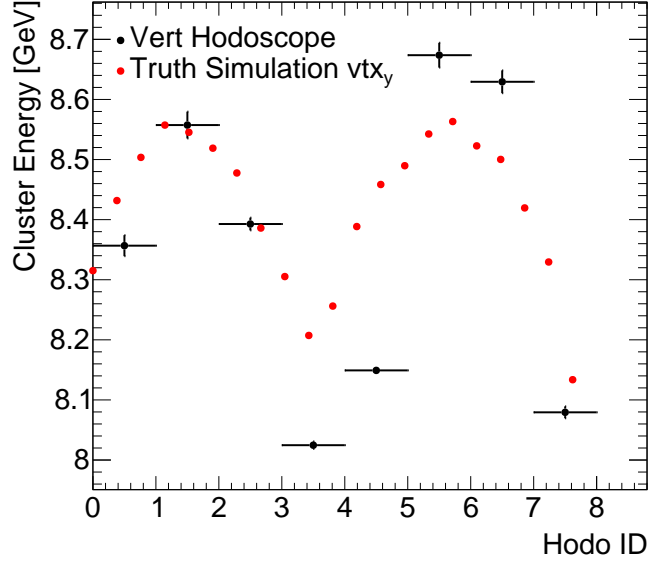


Figure 3.8: Position dependent energy responses in data and simulation are matched together for the purposes of taking a ratio.

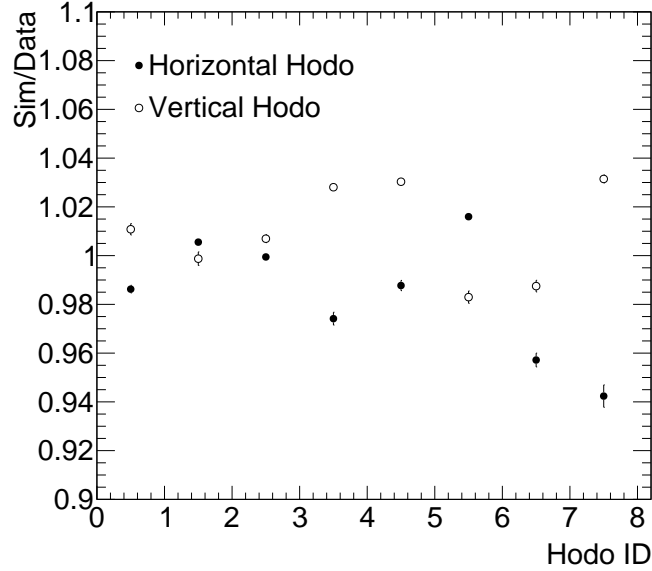


Figure 3.9: The ratio of simulation and data is shown for the position dependent energy response. The ratio is not flat, indicating that significant tuning is required in the simulation to accurately represent the real calorimeters energy response as a function of position.

The mismatch of the data to simulation and the tuning required to remedy this will be discussed further in the results and conclusions section. Already from this study it becomes clear why the resolution measured in simulation in figure 3.2 does not match the resolution measured in the data in the third joint energy scan, figure 2.16 or 2.9. This is because the simulation is not adequately reproducing the position dependence of the energy response in the actual calorimeter. The reason

that the simulation matches the data in the first joint energy scan in figures 2.15 is that this data only is focused on the center of a particular tower, so the effects from the block boundaries are minimized. Thus the realistic implementation of the block boundaries in the simulation is not nearly as important for the first joint energy scan as it is for the third joint energy scan due to the area of the calorimeter that was covered.

4 Results and Conclusions

The final results are shown in this section. Results from the first and third joint energy scan are shown in their respective sections, with the hodoscope position correction and cluster position correction. Simulated curves are based on the simulations described in the previous section. The results indicate that the position dependent correction results in a comparable resolution to the hodoscope position dependent correction, indicating that with simple clustering we can correct for the position dependence of the energy response in the calorimeter. Comparing the first and third joint energy scans indicates some effects of the block boundaries, namely that the resolution degrades even with the hodoscope or position dependent corrections.

4.1 First Joint Energy Scan Results

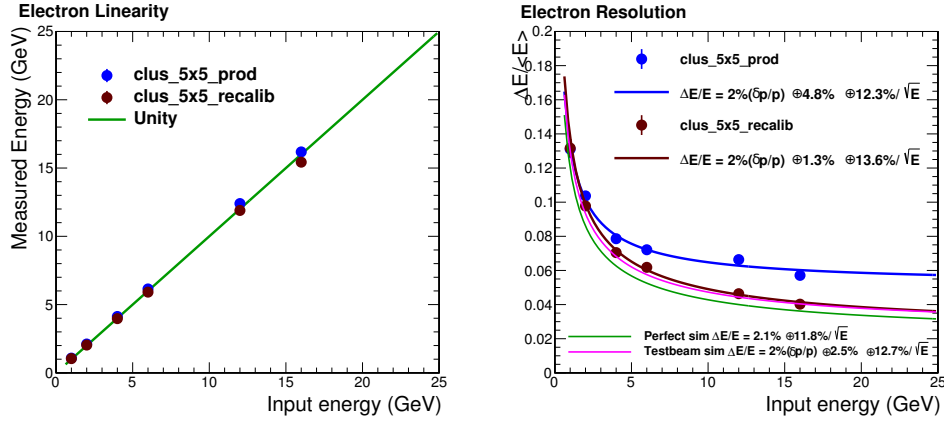


Figure 4.1: The resolution in the first joint energy scan with the application of the cluster position dependent correction is shown. The simulation matches the data well since the effects of block boundaries are minimized due to the beam position.

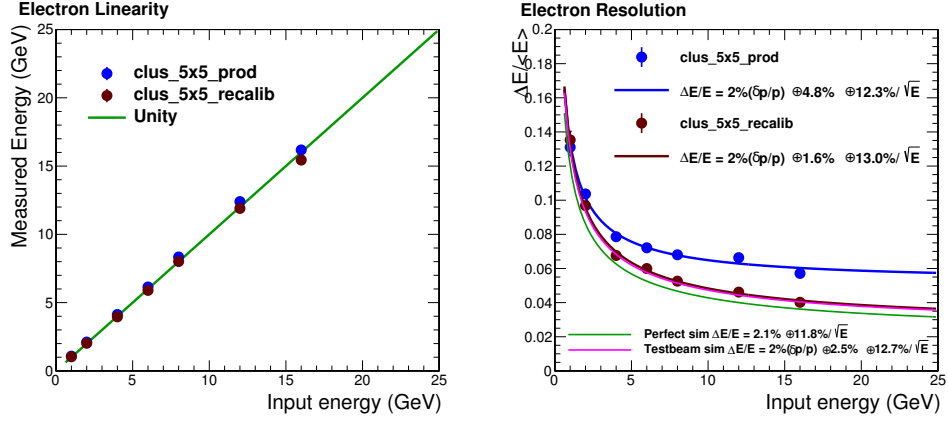


Figure 4.2: The resolution in the first joint energy scan with the application of the hodoscope position dependent correction is shown. The simulation matches the data well since the effects of block boundaries are minimized in these runs.

4.2 Third Joint Energy Scan Results

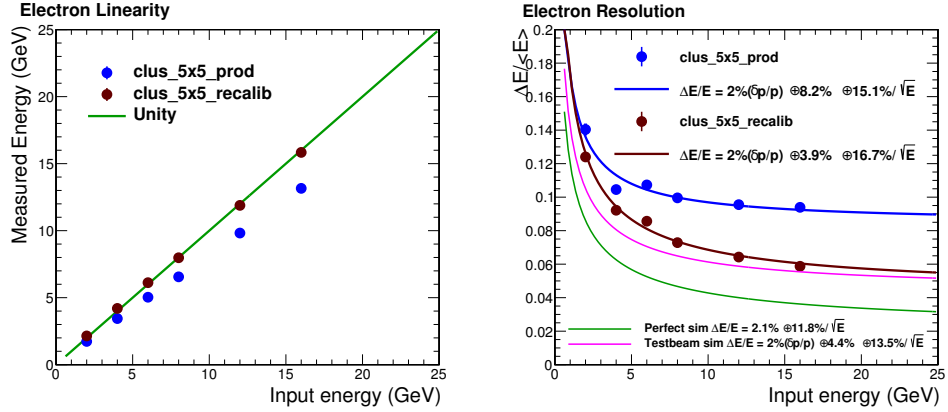


Figure 4.3: The resolution in the third joint energy scan with the application of the cluster position dependent correction is shown. The simulation does not match the data, since the effects of block boundaries are more relevant due to the beam position in the third energy scan.

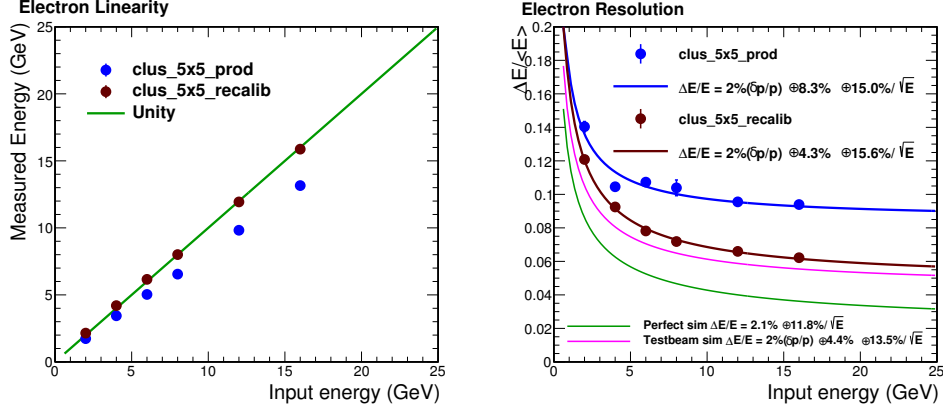


Figure 4.4: The resolution in the third joint energy scan with the application of the hodoscope position dependent correction is shown. The simulation does not match the data, since the effects of block boundaries are more relevant due to the beam position in the third energy scan.

4.3 Conclusions

This note has documented an EMCal analysis for the 2017 T-1044 sPHENIX test beam. In the analysis, electron events were chosen and analyzed to determine the linearity and resolution of the first 2D projective SPACAL EMCal, which will be used in the high rapidity regions of the barrel sPHENIX detector. The analysis focused on two different energy scans, one where the beam was centered on a tower and another where the beam covered a larger area of the calorimeter to determine the effects from the block boundaries. Cluster position and hodoscope position energy dependent response matrices were constructed to improve the resolution of the calorimeter; the cluster position dependent correction is shown to work as well as the hodoscope position correction which was used in Ref. [1]. Simulations were performed to compare to the data, and the simulated resolution agrees well with the data in the first joint energy scan but does not agree with the third joint energy scan.

The simulated position dependent energy responses are shown to clearly not replicate the position dependent energy responses in data. This indicates that additional tuning of the simulation is necessary to replicate the resolution measured in the third joint energy scan, in particular for the block boundary and gaps. While in principle this can be done, it is not a good use of time for several reasons. The blocks that were produced for the 2017 test beam were the first 2D projective towers constructed. Thus, there was still much to learn about the actual construction of the blocks, and consequently the blocks that were produced for the 2017 test beam were known to not be representative of blocks that will be produced for the actual sPHENIX barrel calorimeter. There are already new blocks being constructed for the 2018 test beam, and the knowledge gained from the 2017 block construction has already significantly improved the block construction for the 2018 test beam. These new blocks will likely match the simulation better than what was made for the 2017 test beam, and thus it makes more sense to analyze these to determine the full resolution of the calorimeter since they will be more representative of the full sPHENIX calorimeter. It is thus clear that it is not worth tuning the simulation here to match the block boundaries from 2017 since we know we have better block boundaries on the way for the 2018 test beam which will be more representative of sPHENIX.

The results presented in the first joint energy scan are indicative of the resolution of a particular 2D projective SPACAL tower. Therefore they will by default be better than the resolution covering the entire calorimeter, as shown in the third joint energy scan here or for the data to be taken in the 2018 test beam. A preliminary figure to show publicly is included below, which indicates that the resolution shown is only for a 4x4cm area centered on a particular tower. This is in principle the best possible resolution we can achieve in the 2D towers. One note is that the linearity deviates slightly from unity at low and high energy. In Ref. [1] this was attributed to uncertainty in the actual beam energy at lower energies and leakage out of the back of the EMCal at high energy. At most the linearity deviates by about 2-3% at low/high energy, which is consistent with the 1D blocks that were used in Ref. [1].

4.4 Final Linearity and Resolution

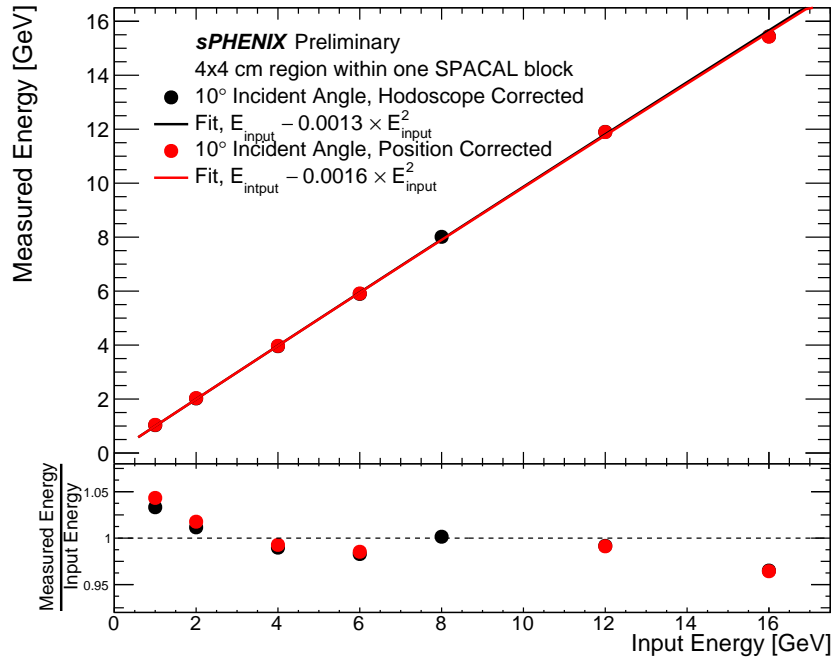


Figure 4.5: Linearity of the EMCal in the first joint energy scan.

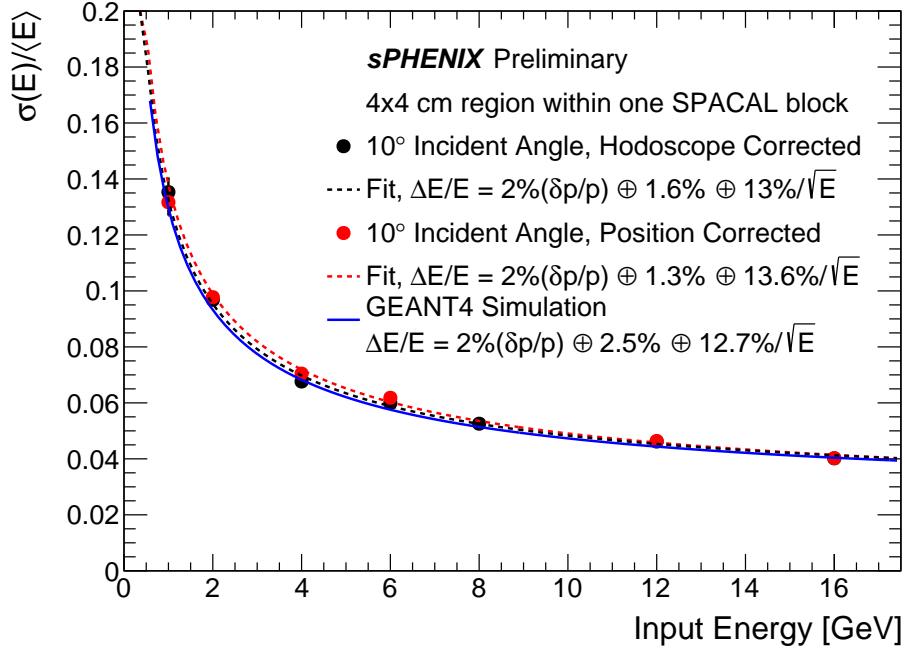


Figure 4.6: Resolution of the EMCal in the first joint energy scan.

References

- [1] C.A. Aidala et al., Design and Beam Test Results for the sPHENIX Electromagnetic and Hadronic Calorimeter Prototypes. arXiv:1704.01461.
- [2] sPHENIX Collaboration.
https://wiki.bnl.gov/sPHENIX/index.php/Position_Dependent_Recalibration_t1044-2017
- [3] sPHENIX Collaboration.
https://wiki.bnl.gov/sPHENIX/index.php?title=T-1044_2017_publication
- [4] sPHENIX Collaboration.
https://wiki.bnl.gov/sPHENIX/index.php/2017_calorimeter_beam_test
- [5] sPHENIX Collaboration.
<https://github.com/sPHENIX-Collaboration/analysis/tree/master/Prototype3/EMCal>.
- [6] sPHENIX Collaboration.
<https://github.com/sPHENIX-Collaboration/coresoftware/tree/master/simulation/g4simulation/g4cemc/>